

## Electrochemical cell for in situ magneto-optic Kerr effect measurements

Kristin M. Poduska and Sylvie Morin

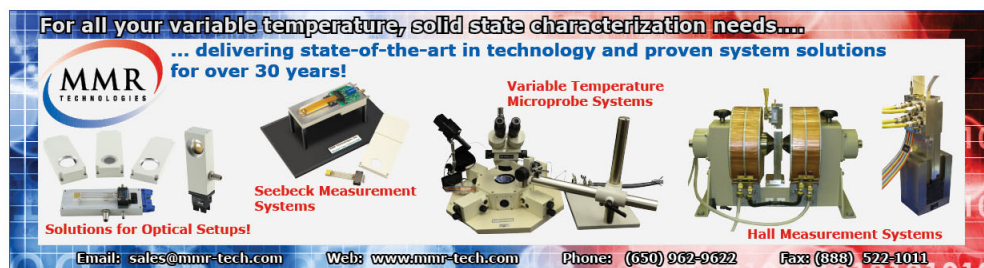
Citation: [Review of Scientific Instruments](#) **74**, 4723 (2003); doi: 10.1063/1.1619583

View online: <http://dx.doi.org/10.1063/1.1619583>

View Table of Contents: <http://scitation.aip.org/content/aip/journal/rsi/74/11?ver=pdfcov>

Published by the [AIP Publishing](#)

---



For all your variable temperature, solid state characterization needs....  
... delivering state-of-the-art in technology and proven system solutions  
for over 30 years!

**MMR**  
TECHNOLOGIES

**Seebeck Measurement Systems**

**Variable Temperature Microprobe Systems**

**Hall Measurement Systems**

Solutions for Optical Setups!

Email: [sales@mmr-tech.com](mailto:sales@mmr-tech.com) Web: [www.mmr-tech.com](http://www.mmr-tech.com) Phone: (650) 962-9622 Fax: (888) 522-1011

# Electrochemical cell for *in situ* magneto-optic Kerr effect measurements

Kristin M. Poduska and Sylvie Morin<sup>a)</sup>

Department of Chemistry, York University, Toronto, Ontario M3J 1P3, Canada

(Received 23 May 2003; accepted 11 August 2003)

A unique electrochemical cell allows *in situ* magneto-optic Kerr effect measurements for magnetic characterization of ultrathin films, concurrently with electrochemical control. This durable, compact, and easy to assemble cell is mounted on a rotatable base which enables magnetic measurements in both the longitudinal (in plane) and polar (perpendicular to plane) configurations. Its utility in the reproducible preparation and *in situ* magnetic characterization of thin films is demonstrated with electrochemical and ferromagnetic hysteresis data for ultrathin Ni films ( $\leq 15$  monolayers) electrodeposited on Ag(111) and Au(111) single crystal substrates. © 2003 American Institute of Physics. [DOI: 10.1063/1.1619583]

## I. INTRODUCTION

There is growing technological interest in applying electrodeposition methods to the synthesis of magnetic multilayer films and nanometer-range structures for data storage and retrieval applications.<sup>1–4</sup> Therefore, property studies of magnetic layers, especially those done *in situ* (under electrochemical control), are of both fundamental and applied importance. To this end, we describe the design of a durable and compact electrochemical cell which enables *in situ* MOKE measurements of ultrathin magnetic films. Its utility is demonstrated through presentation of electrochemical and *in situ* magnetic data for ultrathin Ni films electrodeposited on Ag(111) and Au(111) single crystal substrates.

To date, two techniques have been used to study the *in situ* magnetic responses of ultrathin electrodeposited films [1–20 monolayers (ML)].<sup>5–7</sup> Most recently, ultrathin electrodeposited films have been studied with *in situ* alternating gradient field magnetometry (AGFM), presenting an application of this technique for real time monitoring of deposit magnetization during electrodeposition.<sup>5,6</sup> As the name implies, AGFM uses an alternating field gradient to relate force changes to the sample's magnetization.<sup>8</sup> Prior to these AGFM studies, magneto-optic Kerr effect (MOKE) measurements were used in the report of *in situ* magnetic characterization of electrodeposited elemental films.<sup>7</sup> MOKE measurements exploit the fact that polarized light will change its ellipticity and polarization upon reflection from a magnetic surface as a result of coupling with the magnetic moments of the sample. Thus, it is possible to measure the rotation or ellipticity change as an intensity variation through crossed polarizers. Because this intensity change is directly proportional to the magnetization of the sample, recording the intensity variation as a function of the applied magnetic field will show the traditional hysteretic response of ferromagnetic materials. As with AGFM and other techniques, MOKE methods can be used to measure the anisotropy of a material's magnetic response by changing the relative orientation

of the sample, magnetic field, and plane of the incident and reflected laser beams.

MOKE is an ideal tool for studying the magnetic properties of ultrathin electrodeposits on single crystal substrates. First, MOKE experiments are liquid compatible, provided that the liquid allows sufficient transmission of the incident probe wavelength, so they can be used to assess magnetization behavior of the deposits during an electrochemical experiment.<sup>7</sup> Second, MOKE techniques are effectively surface sensitive in the context of many ultrathin film studies,<sup>9,10</sup> thereby earning the acronym SMOKE (surface MOKE). A light beam in the visible spectrum will penetrate  $\sim 10$ – $20$  nm into most metals near room temperature. Since this depth is substantially greater than the thickness of the electrodeposits described here, MOKE measurements sample the magnetic response through the entire deposit depth. Additionally, nonferromagnetic substrates, such as the noble metals used here, do not affect detection of the electrodeposit's ferromagnetic response. Finally, the experimental geometry of MOKE allows increased flexibility with respect to substrate dimensions and geometry compared to AGFM and other force-based magnetic measurement methods. The primary requirement is a smooth sample surface in order to minimize undesirable light scattering which can reduce the signal-to-noise ratio.

## II. CELL AND CELL-MOUNT DESIGN

The electrochemical cell and mount, shown in Fig. 1, are comprised of components which are nonferromagnetic, and largely nonconducting, to prevent mechanical motion when subjected to large magnetic fields. Additionally, all parts of the cell body are acid resistant to allow thorough cleaning of the cell in a warm sulfuric acid bath prior to each experiment. The cell consists of two adjoining pieces (Fig. 1, A and B) of a rigid, chemically resistant plastic (polytrifluoroethylene, Kel-F), which are joined together using custom-made polyetheretherketon (PEEK) bolts. A 0.16 cm thick (3.8 cm diameter) silica window is positioned between the plastic pieces; grooves in each plastic piece hold a Viton O-ring to ensure a liquid-tight seal between the cell and win-

<sup>a)</sup>Author to whom correspondence should be addressed; electronic mail: smorin@yorku.ca

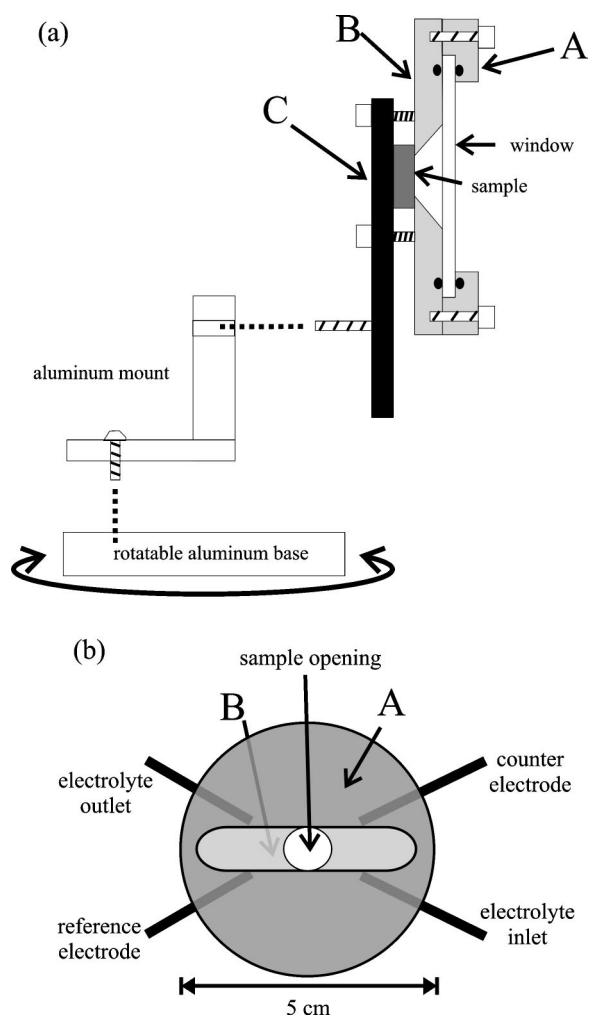


FIG. 1. Schematic drawing of the electrochemical cell designed for *in situ* MOKE measurements. The side view in (a) illustrates the assembly of the plastic cell body (A and B), as well as the support piece (C) which secures the sample and is held in the aluminum mount attached to a rotatable base. The front view of the cell body (b) highlights the inlets for electrolyte, counter electrode, and reference electrode (through B) as well as the slotted front piece (A) which enables optical access to the sample.

dow. Since the plastic cell body is rigid and encases the silica window, the assembled cell is resistant to breakage.

This cell can accommodate samples (working electrode substrates) which are between 8 and 12 mm in diameter and have a thickness of up to 10 mm. The data presented here were obtained using single crystal metal disk substrates, nominally 10 mm in diameter and 3 mm thick; this cell has also been used successfully with gold-coated glass substrates (1 mm thick). In either case, the surface of interest is secured to the opening in the center of the cell [Fig. 1(a), B] with a nonconducting plate [Fig. 1(a), C] made of acetal resin (Delrin). A 0.2 mm thick Teflon spacer (not shown) rests between the sample surface and cell to prevent excessive sample deformation or scratching. External electrical contact to the working electrode is made by placing a thin brass strip between the Delrin spacer and the sample (not shown).

Figure 1(b) highlights features which make the combination of electrochemistry and magneto-optical measurements possible. The front portion of the cell body [Fig. 1(a), A] has a large slot cut out to allow the laser beam to reach,

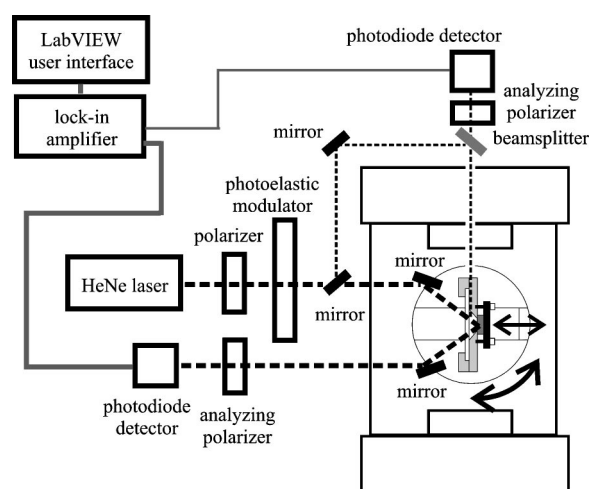


FIG. 2. Schematic depiction of the MOKE setup. The thick dotted lines indicate the optical path of the laser for longitudinal (in-plane) magnetic measurements, while the thin dotted lines correspond to the alternative optical path for polar (perpendicular-to-plane) magnetic investigations. The arrows show the directions in which the electrochemical cell can be rotated and adjusted to facilitate measurements in either configuration.

and be reflected from the sample. The rear portion of the cell body [Fig. 1(b), B] contains a hollow which holds  $\sim 0.5$  mL of electrolyte. The hollow is beveled to ensure that the laser beam has an unimpeded path to the sample surface.

To provide the liquid and electrical junctions necessary for electrochemical control, one part of the cell body has four 1-mm-diameter capillary channels [Fig. 1(a), B]. A pair of capillaries is used for electrolyte inlet and outlet; these are tapered slightly to ensure a good seal between the polytetrafluoroethylene (PTFE) tubing (0.5 mm inner diameter) and the cell body. For the experiments described here, the inlet is connected to one of two electrolyte-containing syringes (Hamilton Gastight) that can be selected via a Teflon-lined valve (Hamilton). A plating electrolyte is added at the beginning of each experiment and can be replenished after deposition. Alternatively, a more acidic stripping electrolyte (0.1 M  $\text{H}_2\text{SO}_4$ ) can be introduced into the cell without disrupting electrochemical control. The remaining two cell capillaries hold the counter electrode (a high-surface-area gold strip, Alfa Aesar Premion) and reference electrode (Ag/AgCl in saturated KCl, made in-house).

With its compact size (5 cm diameter and a thickness near 2 cm), this cell fits easily between the poles of a standard commercially available electromagnet. The adjustable sample mount, shown in Fig. 1(a), enables fine tuning of the cell's position within the magnetic field. The Delrin plate [Fig. 1(a), C] fits in an aluminum mount and is secured with brass bolts in a grooved aluminum base. This mounting scheme allows easy adjustment of sample height and forward/reverse positioning. Moreover, the base rotates to enable longitudinal (in plane) and polar (perpendicular to plane) MOKE measurements on the sample (Fig. 2). For measurements in the polar configuration, the tilt of the sample can be adjusted by a four-point adjustment of the platform on which the rotatable base rests (not shown). In both polar and longitudinal configurations, the grooved base ensures that the cell's lateral position is fixed.

### III. EXPERIMENTAL SETUP

Single crystals of Ag and Au were oriented to their (111) faces within  $0.1^\circ$  using x-ray diffraction methods. Subsequent mechanical polishing, ending with  $0.25\ \mu\text{m}$  diamond paste, yielded an optically smooth surface. To remove embedded polishing debris, the Ag crystals were chemically polished according to a multistep process described elsewhere,<sup>11</sup> while the Au crystals were electropolished several times. Each electropolishing cycle consisted of oxidizing the topmost gold layers by immersion of the crystal face in 1 M  $\text{HClO}_4$  for 2 min while under galvanostatic control at  $0.1\ \text{A}/\text{cm}^2$ , followed by removal of the thin oxide in 1 M  $\text{HCl}$ .<sup>12</sup> Immediately before each deposition experiment, the crystals were subjected to a final surface treatment: additional chemical polishing for Ag crystals, or flame annealing for Au crystals.

Prior to use, the electrochemical cell components were cleaned in warm concentrated  $\text{H}_2\text{SO}_4$ . The crystals were mounted in the (dry) electrochemical cell, and the working electrode potential was maintained for the entire time that the substrate was in contact with the electrolyte. For all experiments described here, the working electrolyte was prepared from high purity starting materials: 10 mM  $\text{H}_3\text{BO}_3$  (BDH Aristar, 99.8% nominal purity), 1 mM  $\text{NiSO}_4$  (Alfa Aesar, Puratronic 99.9985% nominal purity) and 0.1 mM  $\text{HCl}$  (Baseline, Seastar Chemicals) in ultrapure Milli-Q water (Millipore, 2–6 ppb total carbon content, 18.2  $\text{M}\Omega$ ), yielding an electrolyte  $\text{pH}$  near 4.

Potentiostatic control of the working electrode was maintained throughout each experiment using a potentiostat (Hokuto Denko HA-501) regulated by an external function generator (Hokuto Denko HB-104). The measured voltage at and current through the working electrode were digitized (Stanford Research Systems SR810) and recorded with a LabVIEW program (National Instruments) of our design. A Coulombmeter (Hokuto Denko HF-201) measured the total amount of charge passed during deposition. All working electrode potentials are given with respect to a saturated calomel reference electrode (SCE).

Our MOKE measurement apparatus is configured similarly to others described for *ex situ*<sup>13–15</sup> and *in situ*<sup>7</sup> measurements, as shown in Fig. 2. A 1 mW linearly polarized HeNe laser beam (Melles Griot) is polarization modulated at 50 kHz with a photoelastic modulator (Hinds PEM-90) and is incident on the sample near  $60^\circ$  from the sample normal. A Si photodiode detector (Hinds DET-90), preceded by a Glan–Thompson polarizer (Melles Griot), registers the intensity variations of the reflected beam as the sample is subjected to a sweeping magnetic field (GMW electromagnet, Inverpower power supply). These intensity variations are detected with a lock-in amplifier (Stanford Research Systems SR810). The magnetic field control, intensity measurements, and subsequent data analysis are coordinated with LabVIEW programs written in-house. Our setup includes two detectors, one in the polar configuration and one in the longitudinal configuration, so that it is possible to measure both the in-plane and perpendicular magnetization on the same elec-

trode; the only adjustment required is rotation of the cell mount.

### IV. TESTING THE CELL

#### A. Electrochemical deposition and dissolution

Prior to thin film growth, cyclic voltammograms (records of working electrode current as a function of applied potential) were obtained in a potential region where no Ni dissolution or substrate oxidation occurs (here, between  $-0.5$  and  $+0.2\ \text{V}$ ); typical sweep rates were  $20$ – $50\ \text{mV}/\text{s}$ . These current *versus* potential responses are characteristic of the electrolyte composition and  $\text{pH}$ , as well as the crystal face and elemental composition of the substrate. In the absence of an electrochemical reaction, the recorded current corresponds to charging and discharging of the electrochemical double layer. Thus, a cyclic voltammogram (CV) provides a check of surface cleanliness. In these experiments, we also observed additional cathodic current below  $-0.1\ \text{V}$  which was due to reduction of oxygen present in the electrolyte.

Once a characteristic CV was obtained, a thin Ni deposit was formed by applying a single potential step from  $-0.63$  to  $-1.00\ \text{V}$  for a controlled period of time, typically  $10$ – $80\ \text{s}$ . To end the deposition, the potential was stepped back to either  $-0.63$  or  $-0.66\ \text{V}$  for Au or Ag substrates, respectively; the Ni deposit neither grows nor dissolves significantly at these resting potentials. After characterizing the magnetic response of the deposit (described in the next section), its effective thickness was assessed using stripping voltammetry. Integration of the area under the anodic dissolution peak gave the total amount of charge passed. Given the nominal surface area of the deposit ( $0.33\ \text{cm}^2$ ), and assuming a (111) arrangement of Ni with an atomic spacing equal to the Ni bulk value ( $2.49\ \text{\AA}$ ), the effective coverage was calculated directly from the area of the dissolution peak ( $1\ \text{ML} = 590\ \mu\text{C}/\text{cm}^2$ ). Our experience has shown that a more acidic electrolyte is necessary to remove films that become slightly oxidized during the course of the experiment, perhaps due to the presence of residual oxygen in the cell or changes in the  $\text{pH}$  near the working electrode surface during the deposition process. Flushing out the Ni-based electrolyte and replacing it with an electrolyte with a lower  $\text{pH}$  ( $0.1\ \text{M}\ \text{H}_2\text{SO}_4$ ), while adjusting the working electrode potential slightly to maintain a safe resting potential, consistently enabled complete film dissolution in a single sweep.

Representative dissolution curves for Ni films deposited at  $-1.0\ \text{V}$  are shown in Fig. 3. In each case, the Ni dissolution charge ( $Q_{\text{dis}}$ ) was less than the total charge passed during Ni deposition ( $Q_{\text{dep}}$ ). This is to be expected since there is hydrogen coevolution during the deposition process. The current efficiency ( $Q_{\text{dis}}/Q_{\text{dep}}$ ) for Ni deposition at  $-1.0\ \text{V}$  in the specified electrolyte is  $\approx 60\%$ . Effective coverages for deposition times between  $10$  and  $80\ \text{s}$  at  $-1.0\ \text{V}$  are shown in Fig. 4, wherein each data point represents the average of several separate experiments. For deposition times  $\leq 30\ \text{s}$ , the effective Ni coverage increases linearly with deposition time, corresponding to a deposition rate of  $\sim 0.33\ \text{ML}/\text{s}$ . Figure 4(b) emphasizes the linear relation between coverage and



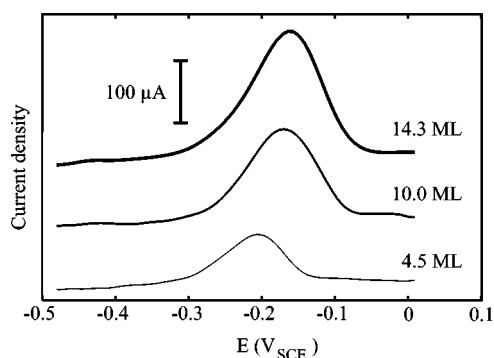


FIG. 3. Comparison of dissolution curves of Ni/Ag(111) obtained for different deposition times. All curves were obtained with a sweep rate of 8 mV/s. The plots are staggered in the y direction for clarity, but the relative magnitudes are preserved. The effective coverage resulting from peak integration is noted next to each curve in the figure. In each case shown here, the error associated with calculating the peak area was  $\pm 0.2$  ML.

the square root of the deposition time, indicating diffusion-limited growth for longer deposition times. We note that this is not an artifact of the cell design, since similar behaviors are typically observed in more traditional, larger volume electrochemical cells when the electrolyte is not agitated by stirring or sample rotation.

### B. *In situ* magnetic characterization

After depositing the Ni films (in the absence of an applied magnetic field), the magnetic response of the electrode-

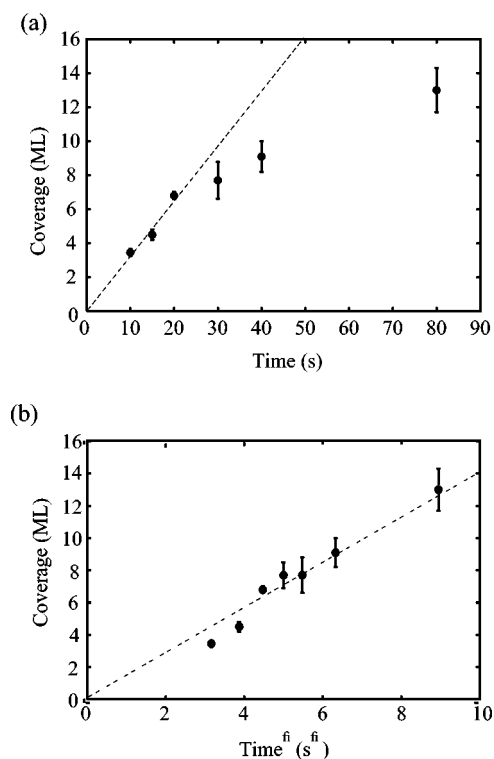


FIG. 4. Effective coverage as a function of deposition time (at  $-1.00$  V) for Ni/Ag(111). For deposition times between 10 and 30 s, coverage increases approximately linearly with increasing deposition time, shown in (a). A linear least-squares fit of data within this time interval, denoted by the dotted line, yields a deposition rate of  $\sim 0.33$  ML/s. The linear relationship between coverage and the square root of the deposition time, (b), confirms film growth is limited by diffusion. Error bars correspond to the variation in film thickness from among different experiments, which is better than 10% even for the thickest films studied.

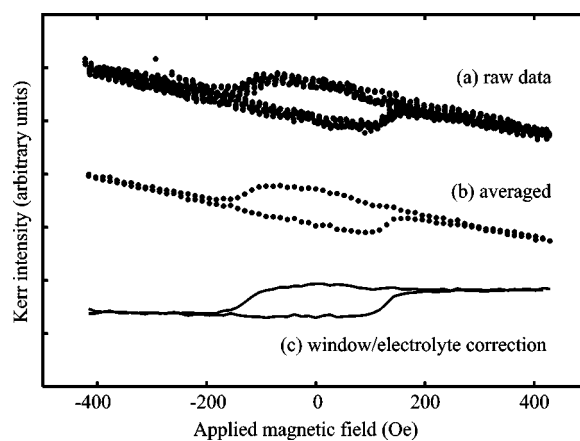


FIG. 5. Series of curves to show the data treatment procedure for magnetic hysteresis loops obtained from *in situ* MOKE measurements. The raw data in (a) include four successive hysteresis loops from a  $14.3 \pm 0.2$  ML Ni film on a Ni/Ag(111) surface. These loops are averaged, using 13 Oe bins, to improve the signal to noise ratio as shown in (b). Finally, the data are corrected for contributions from the aqueous electrolyte and the cell's silica window, using a linear regression fit of the magnetic saturation regions at the most extreme magnetic field values, to yield the final hysteresis curve shown in (c). All hysteresis curves presented here were treated in a similar manner.

posit was characterized using the MOKE technique. Each hysteresis loop was recorded while the sample was at an appropriate resting potential. Laser light was directed onto the sample while sweeping the magnetic field at a slow rate ( $5\text{--}20$  Oe/s), typically between  $\pm 400$  Oe. The resulting light intensity changes were recorded as a function of the applied magnetic field. To improve the signal to noise ratio, two to eight consecutive scans were averaged. Figure 5 provides a comparison of typical raw hysteresis data [Fig. 5(a)] and their average [Fig. 5(b)]. The light intensity values for these four successive scans were averaged using a bin size that was comparable to the steps in the applied magnetic field used during the scan. Finally, the data were corrected for contributions from the aqueous electrolyte and the cell's silica window [Fig. 5(c)] using a linear regression fit of the saturated magnetic regions at the most extreme magnetic field values. All hysteresis curves presented here were treated in a similar manner.

Representative hysteresis loops for Ni films between 4 and 15 ML are shown in Fig. 6. The in-plane magnetization component showed an increase in coercivity with increasing film thickness. No perpendicular magnetization was detected, as shown in Fig. 6(b). Despite the absence of perpendicular hysteresis behavior, a field-dependent contribution from the cell's silica window and the electrolyte was clearly visible in the raw data. This field-dependent contribution exhibited a signal-to-noise ratio that was comparable to that observed in raw data obtained in the longitudinal configuration, such as that presented in Fig. 5. Therefore, we conclude that the electrochemical cell and the MOKE setup function properly in the polar configuration. Furthermore, other studies have reported that Ni films display predominantly in-plane magnetic behavior, whether electrodeposited on Au(111)<sup>5</sup> or prepared under UHV conditions on Ag(111).<sup>16</sup> Thus, our observations are in agreement with these findings.

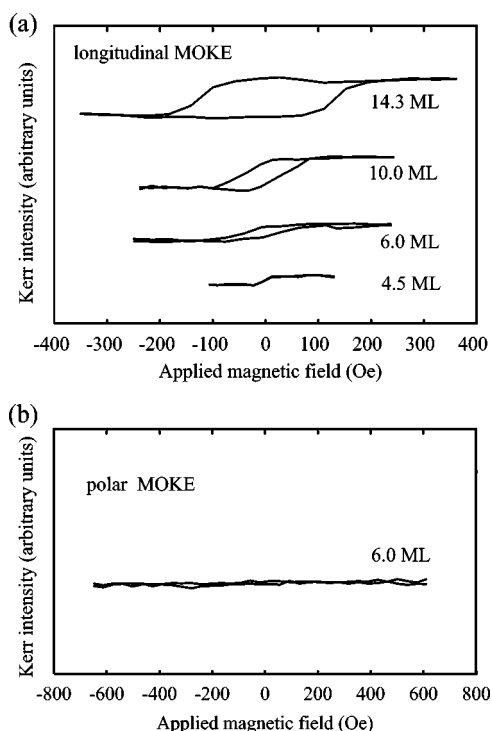


FIG. 6. Ferromagnetic response of Ni/Ag(111) after different deposition times at  $-1.00$  V, in the absence of a magnetic field. The in-plane hysteresis loops (longitudinal MOKE configuration) shown in (a) were recorded at  $-0.66$  V, at which potential the deposit displays no substantial growth or decay. Data were averaged over two to eight consecutive scans and then corrected for diamagnetic contributions from the aqueous electrolyte and silica window. Perpendicular magnetization was not observed for Ni/Ag(111); (b) is a representative MOKE scan in the polar configuration, obtained from the same 6.0 ML film as shown in (a). In each case shown here, the error estimate for coverage was  $\pm 0.2$  ML.

The *in situ* cell does not limit the sensitivity of our MOKE measurements; the signal-to-noise ratio compares favorably with previously reported data for electrodeposited films of similar thickness.<sup>5,15</sup>

With these electrochemical and magnetic data, we demonstrate the utility of our new electrochemical cell design for *in situ* magnetic measurements. Its compact size and rotatable base make it ideal for studies of both in-plane and perpendicular magnetization.

## ACKNOWLEDGMENTS

This work was possible thanks to funding from the Natural Science and Engineering Research Council (Canada), the Canada Foundation for Innovation, and the Ontario Innovation Trust. S.M. acknowledges support from the Canada Research Chair Program and York University. We also gratefully acknowledge the support and expertise of Dr. P. Norton, Dr. L. Coatsworth, and R. Barbeito at the University of Western Ontario (Canada) in the initial phases of this project, as well as I. Moore (York University Machine Shop).

- <sup>1</sup>C. A. Ross, *Annu. Rev. Mater. Sci.* **24**, 159 (1994).
- <sup>2</sup>W. Schwarzhacher and D. S. Lashmore, *IEEE Trans. Magn.* **32**, 3133 (1996).
- <sup>3</sup>S. Araki, M. Sano, S. Li, Y. Tsuchiya, O. Redon, T. Sasaki, N. Ito, K. Terunuma, H. Morita, and M. Matsuzaki, *J. Appl. Phys.* **87**, 5377 (2000).
- <sup>4</sup>T. Osaka, *Electrochim. Acta* **45**, 3311 (2000).
- <sup>5</sup>A. Gündel, L. Cagnon, C. Gomes, A. Morrone, J. Schmidt, and P. Allongue, *Phys. Chem. Chem. Phys.* **3**, 3330 (2001).
- <sup>6</sup>A. Gündel, A. Morrone, J. E. Schmidt, L. Cagnon, and P. Allongue, *J. Magn. Magn. Mater.* **226**, 1616 (2001).
- <sup>7</sup>W. Schindler and J. Kirschner, *Rev. Sci. Instrum.* **67**, 3578 (1996).
- <sup>8</sup>P. Flanders, *J. Appl. Phys.* **63**, 3940 (1988).
- <sup>9</sup>S. D. Bader, *J. Magn. Magn. Mater.* **100**, 440 (1991).
- <sup>10</sup>Z. Q. Qiu and S. D. Bader, *Rev. Sci. Instrum.* **71**, 1243 (2000).
- <sup>11</sup>T. Kurasawa, *Chem. Abstr.* **55**, 14279 (1961).
- <sup>12</sup>K. Engelsmann and W. J. Lorenz, *J. Electroanal. Chem.* **114**, 1 (1980).
- <sup>13</sup>S. N. Jasperson and S. E. Schnatterly, *Rev. Sci. Instrum.* **40**, 761 (1969).
- <sup>14</sup>L. Cagnon, T. Devolder, R. Cortes, A. Morrone, J. E. Schmidt, C. Chappert, and P. Allongue, *Phys. Rev. B* **63**, 104419 (2001).
- <sup>15</sup>J. R. Hampton, J.-L. Martínez-Albertos, and H. D. Abruña, *Rev. Sci. Instrum.* **73**, 3018 (2002).
- <sup>16</sup>C. A. Ballentine, R. L. Fink, J. Araya-Pochet, and J. L. Erskine, *Appl. Phys. A: Solids Surf.* **49**, 459 (1989).